

Multi-Thread Hydrodynamic Modeling of a Solar Flare

Harry P. Warren

*E. O. Hulburt Center for Space Research, Code 7670, Naval Research Laboratory, Washington,
DC 20375
hwarren@nrl.navy.mil*

ABSTRACT

Past hydrodynamic simulations have been able to reproduce the high temperatures and densities characteristic of solar flares. These simulations, however, have not been able to account for the slow decay of the observed flare emission or the absence of blueshifts in high spectral resolution line profiles. Recent work has suggested that modeling a flare as an sequence of independently heated threads instead of as a single loop may resolve the discrepancies between the simulations and observations. In this paper we present a method for computing multi-thread, time-dependent hydrodynamic simulations of solar flares and apply it to observations of the Masuda flare of 1992 January 13. We show that it is possible to reproduce the temporal evolution of high temperature thermal flare plasma observed with the instruments on the *GOES* and *Yohkoh* satellites. The results from these simulations suggest that the heating time-scale for a individual thread is on the order of 200 s. Significantly shorter heating time scales (20 s) lead to very high temperatures and are inconsistent with the emission observed by *Yohkoh*.

Subject headings: Sun: corona, Sun: flares

1. Introduction

Solar flares are a potentially rich source of information on how energy is released during magnetic reconnection. At present, however, our physical understanding of solar flares is largely qualitative. Solar flare models based on magnetic reconnection are broadly consistent with observations, but detailed comparisons between numerical models and observations have been generally unsuccessful. For example, most previous attempts to model solar flares with time dependent hydrodynamic simulations have not been able to account for essential aspects of the observations, such as the evolution of the observed emission or the details of the spectral line profiles (e.g., Peres et al. 1987; Mariska & Zarro 1991). Hydrodynamic simulations indicate that high density flare plasma cools rapidly, while soft X-ray emission from solar flares often persists for many hours. Hydrodynamic simulations also predict that high velocity upflows should be observed during the impulsive phase of the flare. In the vast majority of observed line line profiles, however, the stationary component is dominant (e.g., Mariska et al. 1993)

One difficulty with most previous hydrodynamic modeling efforts is that they have treated the flare as a single loop. This is clearly inconsistent with observations taken at high spatial resolution which show that solar flares are not the result of depositing energy into a single loop. Rather, these observations suggest that solar flares are composed of many small-scale threads (e.g., Warren et al. 1999; Warren 2000; Aschwanden & Alexander 2001). Furthermore, flare observations also show that plasma at many different temperatures is present simultaneously indicating that these threads are not all heated at once, but over the duration of the event.

Some recent work has attempted to incorporate this observational understanding of magnetic reconnection into hydrodynamic simulations and model flares as a superposition of many independently heated threads. Hori et al. (1997, 1998), for example, found that the spatially averaged line profiles resulting from a succession of independently heated loops will generally be dominated by the stationary component, in qualitative agreement with observations. However, they were not able to perform detailed comparisons with observations. Using a similar approach Reeves & Warren (2002) were able to model the temporal evolution of emission at both high temperatures (~ 10 MK) and relatively cool temperatures (~ 1 MK) during the rise phase of an event. Some discrepancies between the simulation and the observations were evident, however, during the decay of the event they modeled. This work also did not use full solutions to the hydrodynamic loop equations, rather they employed the Cargill et al. (1995) scaling laws to approximate the evolution of the plasma.

Treating a flare as a succession of threads introduces additional complexities into the hydrodynamic modeling. Since the observed emission results from the superposition of many threads it is not obvious how to determine the properties of an individual thread. Recently, Warren & Doschek (2005) have shown how to use *GOES* soft X-ray fluxes to derive the energy flux and volume for each thread using a minimum of assumptions. This algorithm allows for detailed comparisons between a multi-thread, time-dependent hydrodynamic simulation and observations. For the Ca XIX and S XV resonance lines they found generally good agreement for both the intensity and the line profiles observed during the initial phase of a flare. They found that the strongly blue-shifted emission evident during the initial heating of a thread is largely masked by threads that have been heated previously and do not show bulk motions. The extended lifetime of the flare relative to a characteristic cooling time was easily reproduced using a succession of threads.

In this paper we present a detailed description of the algorithm for computing a multi-thread, time-dependent hydrodynamic simulation of a solar flare. We apply this modeling to a well studied event, the Masuda flare of 1992 January 13 (e.g., Masuda et al. 1995). Our focus here is on the evolution of the thermal emission observed with the Soft X-Ray Telescope (SXT), the Bragg Crystal Spectrometer (BCS), and Hard X-Ray Telescope (HXT) instruments on *Yohkoh*. Of particular interest is the evolution of the BCS Fe XXV and HXT light curves. Emission observed in these channels is formed at very high temperatures and is likely to be the most sensitive to the details of the energy deposition during the flare.

2. Observations

The Masuda flare was a *GOES* M2.0 flare that occurred on the west limb of the Sun on 1992 January 13. As is shown in Figure 1, the event began at about 17:22, peaked at about 17:33, and decayed slowly over the next two hours. This flare was well observed by the instruments on the *Yohkoh* spacecraft. The *Yohkoh* instruments include the Soft X-ray Telescope (SXT, Tsuneta et al. 1991), the Bragg Crystal Spectrometer (BCS, Culhane et al. 1991), and the hard X-ray telescope (HXT, Kosugi et al. 1991).

The soft X-ray images from SXT for this event are shown in Figure 1. These images suggest a simple rising, two-ribbon flare arcade structure. The height of the arcade moves up by about $7''$ during the time the SXT images are available (from approximately 17:26 to 17:42). Aschwanden et al. (1996) estimate the radius for the soft X-ray emission to be 12,500 km at 17:28, which corresponds to a total loop length of about 39 Mm.

The emission in the lowest energy HXT channel (L 14–23 keV) is generally co-spatial with the loops imaged with SXT, indicating that the emission in this energy range is predominately thermal in origin. At higher energies (M1 23–33 keV and M2 33–53 keV) the emission emanates from the loop footpoints and a relatively weak source above the arcade (e.g., Masuda et al. 1995). Additional hard X-ray observations of the Masuda flare are available from the BATSE instrument on the *Compton Gamma Ray Observatory (CGRO)*. From these data Aschwanden et al. (1996) compute a spectral index of $\gamma = 3.74$ for the 30–120 keV energy range near the peak of the hard X-ray emission.

SXT filter ratios suggest temperature in the range of 10–12 MK in the brightest regions of the arcade. SXT also indicates a region of elevated temperatures (~ 20 MK) in the faint region slightly above the arcade (e.g., Doschek et al. 1995; Tsuneta et al. 1997). BCS spectra, such as those shown in Figures 2, indicate peak temperatures ranging from about 17 MK (S XV) to 20 MK (Fe XXV). The differences between the temperatures derived from SXT and BCS suggest that the flare arcade is multi-thermal (Doschek et al. 1995). Using the BCS fluxes in combination with spatially integrated SXT intensities yields emission measure distributions consistent with multi-thermal plasma (McTiernan et al. 1999).

3. Single Loop Hydrodynamic Simulations

To illustrate the difficulties with previous solar flare hydrodynamic simulations we consider the modeling of the Masuda event as a single loop. We simulate the flare using the Naval Research Laboratory solar flux tube model (e.g., Mariska 1987) and the electron beam formalism of Mariska

et al. (1989). The injected electron spectrum is assumed to be of the form

$$F_{in}(E_0, t) = \frac{4(\delta - 2) F_{max} g(t)}{\delta + 2} \frac{1}{E_c^2} \begin{cases} \left(\frac{E_0}{E_c}\right)^2, & E_0 \leq E_c, \\ \left(\frac{E_0}{E_c}\right)^{-\delta}, & E_0 \geq E_c. \end{cases} \quad (1)$$

Here E_c is the low-energy cutoff, F_{max} is the energy flux injected into the loop, and $g(t)$ is the temporal envelope on the heating. For thick target bremsstrahlung δ is related to the spectral index (γ) of the observed non-thermal emission by $\delta = \gamma + 1$ (Tandberg-Hanssen & Emslie 1988). We use the loop length inferred from the observations and a spectral index of $\delta = 4$ to approximate the observations. Note that the energy deposition can be expressed as an analytic function of the integrated column density when δ is an even positive integer. We use a triangular envelope with a width of 80 s that fits, at least approximately, the observed hard X-ray profile at the higher energies.

The only adjustable parameters in the simulation are the low-energy cutoff, the energy flux injected into the loop, and the cross-sectional area of the loop. For a fixed value of E_c the injected energy flux and the loop area are constrained by the need to reproduce the magnitude of both *GOES* soft energy fluxes. In Figure 3 we show the results from a simulation with $E_c = 10$ keV, $F_{max} = 3 \times 10^{10}$ ergs cm⁻², and a total volume of 2.8×10^{27} cm³. The densities and temperatures computed from the simulation have been convolved with the *GOES* temperature response to compute the expected emission in each channel as a function of time. From this comparison it is clear that a single loop model will have a difficult time reproducing the observed emission. In the observations there is a delay of about 240 s between the peak of the hard X-rays and the peak of the soft X-ray emission. The observations also show a very slow decline in the soft X-ray emission. The simulated light curves, in contrast, show both a rapid increase and a rapid decay, suggesting that the soft X-ray emission is very sensitive to the energy deposition.

It is tempting to posit that modifications to the heating function assumed in this exercise would improve the agreement between the observations and the numerical simulation. Variations in the spectral index or in the low energy cutoff, for example, would change the observed light curves. It is also possible to abandon the requirement that the heating be solely due to precipitating electrons and superimpose a second, more slowly varying heating on the loop. In particular, several previous studies have considered the role of extended heating in explaining the decay of the soft X-ray emission (e.g., Reale et al. 1997). It is clear from the observations, however, that extended heating during the decay phase cannot be the primary cause of the extended life-time of the soft X-ray emission. In this event, for example, the first H α post-flare loops appear at 17:38 UT (Wang et al. 1995) when, as is indicated by the *GOES* light curves and the *SXT* images, the high temperature soft X-ray emission is still substantial. Furthermore, these H α loops appear at heights below the soft X-ray loops observed with *SXT*. It is unambiguous that single loop modeling cannot account for the observed evolution of the flare arcade. This conclusion has been reached by other authors (e.g., Moore & Labonte 1980; Svestka et al. 1982; Schmieder et al. 1995). This understanding, however, has not been widely incorporated into the hydrodynamic modeling of solar flares.

4. Multi-Thread Hydrodynamic Modeling

One impediment to modeling a solar flare as the succession of independently heated threads is the difficulty in determining the heating parameters for each thread. The observables from a flare, such as the *GOES* soft X-ray fluxes, are typically used to compute physical properties of the flare arcade, such as the temperature and emission measure. These quantities are difficult to use as inputs to a hydrodynamic simulation.

Recent work by Warren & Antiochos (2004) has investigated the relationship between the *GOES* soft X-ray fluxes and the parameters relevant to hydrodynamic simulations, such as the total energy deposited into a thread and the volume of the thread. They found that the peak fluxes in the *GOES* channels were related to the energy input into the loop by

$$F_{1-8}(t_P) \simeq 3.68 \times 10^{-35} \left[\frac{EL}{V} \right]^{1.75} \frac{V}{L^2} \quad (2)$$

and

$$F_{0.5-4}(t_P) \simeq 4.42 \times 10^{-42} \left[\frac{EL}{V} \right]^{2.24} \frac{V}{L^2}. \quad (3)$$

Here E is the total energy deposited in the loop, L is the total loop length, and V is the loop volume. The cross-sectional area (A) is V/L . Conceptually, we can think of the hydrodynamic loop equations as describing the evolution of the plasma in a thin, semi-annular volume where the loop length corresponds to the semi-diameter.

Assuming that the loop length can be determined independently, equations 2 and 3 can be inverted to express the energy deposition (E) and loop volume (V) in terms of the peak *GOES* soft X-ray fluxes. These expressions, however, describe the relationship between E , V , and the *GOES* soft X-ray fluxes for a single thread. In our multi-thread simulation we model the flare as a succession of independently heated threads. To account for the contribution of threads that have been heated previously and are cooling we compute the “residual” *GOES* flux for each channel,

$$\Delta F^i(t_p) = \left[F_{obs}(t + t_c) - \sum_{j=1}^{i-1} F_{sim}^j(t + t_c) \right]. \quad (4)$$

Here t_c is essentially the conductive cooling time (the time at which the emission measure of the thread will reach its maximum value). This offset reflects the fact that there will be a delay between the introduction of a thread and the time when it reaches its maximum emission in soft X-rays. In the model t_c is estimated from the simulation of the previous thread. For each thread after the first, the residual *GOES* fluxes are used to compute the energy and volume for the thread.

Computing a multi-thread simulation of a solar flare involves the following steps

1. Using background subtracted *GOES* fluxes we compute the energy and volume needed to reproduce the observed soft X-ray emission.

2. We perform a time-dependent hydrodynamic simulation using the energy derived from the *GOES* data.
3. Calculate the evolution of the *GOES* fluxes from the hydrodynamic simulation and the thread volume derived from the observations.
4. Compute the residual *GOES* flux in each channel, which are then used in step 1 for the next thread in the simulation

In principal, the scaling laws presented in Equations 2 and 3 can be used to approximate the input energy and volume for a thread from the observed *GOES* soft X-ray fluxes. However, these scaling laws are not useful for computing the temporal evolution of a thread and cannot be used to determine the residual fluxes that are important in the determining the parameters for the next thread in the simulation. Thus the use of the scaling laws necessitates that the simulations must be run in series, making the process of simulating a flare very time consuming.

To allow for parallel processing we compute a series of full hydrodynamic simulations using a wide range of input energies. For each of these simulations we calculate the evolution of the *GOES* fluxes in both channels. An illustration of this calculation is shown in Figure 4. With this “grid” of solutions we can interpolate to find the energy and volume needed to reproduce the observed *GOES* fluxes. Additionally we can interpolate in time to estimate the evolution of the thread as it would be observed with *GOES*. The use of interpolated light curves allows for the hydrodynamic simulation parameters for all of the threads to be determined very rapidly. Once the simulation parameters have been determined from the interpolated light curves the full hydrodynamic simulations can be performed in parallel, leading to a dramatic increase in computational efficiency.

Since the scaling laws incorporate significant approximations that are not present in the solutions to the hydrodynamic equations, the use of interpolated light curves makes the flare simulations considerably more accurate. It is also important to note that the scaling laws have not been thoroughly compared with results from hydrodynamic simulations. Warren & Antiochos (2004) only considered variations in the input energy for a single loop length. As illustrated in Figure 4, the scaling laws appear to work well for very short loops. Longer loops are likely to be more problematic. More exhaustive comparisons are currently in progress and will be reported in a future publication.

For this work we make two simplifying assumptions. First, we assume that the threads are heated directly and that energy transport during the initial phase of the flare is dominated by thermal conduction. The functional form of the heating is assumed to be

$$E_H(s, t) = E_0 + g(t)E_{Flare} \exp \left[-\frac{(s - s_0)^2}{2\sigma_s^2} \right], \quad (5)$$

where s_0 designates the location of the impulsive heating, σ_s is the spatial width of the heating, and E_{Flare} is a constant that determines the maximum amplitude of the heating. The background

heating parameter, E_0 , is chosen so that the equilibrium atmosphere is very cool (~ 0.5 MK) and tenuous and has little effect on the evolution of the loop. A more realistic treatment of the energy deposition would include the contribution of energetic particles precipitating into the chromosphere. Figure 3, however, suggests that energetic particle precipitation is responsible for only a small fraction of the observed *GOES* emission during this flare.

The second simplifying assumption is that a fixed loop length can be used for all of the hydrodynamic simulations. The SXT observations indicate that the height of the arcade increases by about 25% during the time that SXT images are available (17:28–17:40 UT). Changes in the loop length of this magnitude do not dramatically alter the evolution of a thread. Incorporating changes in the loop length would require the calculation of a 2 dimensional grid of solutions where both the energy and the loop length are varied. This would add significant computation to the simulation. Also, since there are SXT images only near the peak of the event we have no way to estimate the variation in loop length during most of the decay. For the simulations of this flare we fix the loop length for each thread at 39 Mm. All of the simulations shown in Figure 4 are computed with this loop length and the heating function described by Equation 5.

The hydrodynamic simulations yield the temperature and density along the length of each thread in the arcade. This allows us to compute the emission for any wavelength range in the solar spectrum that is dominated by optically thin emission. For this paper we focus on computing light curves for the HXT, BCS, and SXT instruments on *Yohkoh*. For SXT and HXT we use the standard *SolarSoft* routines `SXT_FLUX` and `HXT_THCOMP` to compute the response as a function of temperature. For BCS we compute synthetic spectra over a wide range of temperatures using `BCS_SPEC` and sum over the resonance line as indicated in Figure 2 to determine the response as a function of temperature. The response curves shown in Figure 5 illustrate how these instruments span the temperature range from approximately 2 MK to above 100 MK.

It is encouraging to note that many of the significant parameters in the multi-thread simulation are derived from the observations and are not adjustable. The energy deposited into each thread and the volume of each thread are inferred from the observed *GOES* fluxes. The loop length can generally be determined from image data, although projection effects can be difficult to account for. There are, however, several parameters in the simulations that are potentially unconstrained by the *GOES* observations, such as the rate at which threads are introduced into the flare arcade. Similarly, the details of the energy deposition, such as its magnitude, duration, and spatial scale, are also largely unconstrained by the *GOES* observations. The peak fluxes are largely determined by the total energy deposited in the loop (e.g., Winebarger & Warren 2004). Additionally, it should not be forgotten that there are a number of simplifying assumptions incorporated into the hydrodynamic simulations. The model chromosphere used in the hydrodynamic code, in particular, is highly simplified.

5. Multi-Thread Hydrodynamic Simulations

An example of a multi-thread simulation for the Masuda flare is shown in Figure 6. In this simulation we have used 50 threads each introduced 40 s apart. For each thread the hydrodynamic code was run using the heating function given in Equation 5 with $\sigma_H = 10^8$ cm, s_0 set equal to the loop apex, and with $g(t)$ a triangular envelop with a width of 200 s. As noted previously we have fixed the loop length at 39 Mm and we focus our attention on the rise phase and beginning of the decay of the flare.

The results presented in Figure 6 indicate that the simulation reproduces the flux in each *GOES* channel very well. The differences between the observed and simulated light curves are typically about 20%. This good agreement is expected since the parameters for each thread were inferred from the *GOES* soft X-ray measurements. The observations from HXT, BCS, and SXT on *Yohkoh* are not used to infer the simulation parameters and offer an independent assessment of the simulation results. The *Yohkoh* instruments also cover a wider range of temperature than the two *GOES* channels. The light curves shown in Figure 6 show that the simulation does a credible job of reproducing the observed *Yohkoh* fluxes. In this flare the highest temperature emission (e.g., HXT L and BCS Fe XXV) peaks earliest and decays quickly while the lower temperature emission (e.g, BCS S XV and SXT Al.1) peaks later and decays relatively slowly, a trend that is observed in many flares (e.g, Sterling et al. 1997). The simulations do a particularly good job of reproducing this behavior.

The most significant discrepancy between the simulation and the observations is for the HXT L and M1 channels very early in the event. At these times the emission in these HXT channels is likely to be non-thermal bremsstrahlung produced by precipitating high energy electrons. At present this modeling only accounts for the thermal emission in a flare. Since the observed BCS Fe XXV light curve is well matched by the simulation it does not appear that the discrepancies in the HXT light curves is caused by the simulation underestimating the temperature.

The modeled SXT light curves generally reproduce the temporal evolution of the observations. The observed SXT fluxes, however, are systematically higher than the simulated fluxes by about a factor of 2. Since this discrepancy is systematic, it may be due to inconsistencies in the radiometric calibration between *GOES* and SXT.

Note that for these comparisons we have subtracted the first flux measurements from the BCS observations to account for the background. This correction is significant only for the BCS S XV emission. For HXT we have estimated the background using fluxes from a period late in the flare. The SXT data during this orbit cover only a small period near the peak of the flare and background subtraction is not possible, and this contributes to the discrepancies between the observation and simulation in these filters.

The energies and volumes for each thread in the simulation are shown in Figure 7. Also shown are the average energy flux (E/A) and the energy density (E/V) for each thread. These quantities

are computed by dividing the total energy input into the thread by the area or the volume of the thread. The equations presented in Section 4 suggest that the peak temperatures and densities in each thread are largely determined by the energy flux. Thus the largest energy fluxes occur early in the flare and generally correspond to those threads which have the highest peak temperatures and densities. The maximum *GOES* ratio of 0.25 occurs at about 17:29 UT, close to the peaks in the HXT L and BCS Fe XXV emission. After this time the flux in the 0.5–4 Å channel declines more rapidly than the flux in the 1–8 Å channel, suggesting declining peak temperatures and therefore declining energy fluxes. Solving Equations 2 and 3 for the energy flux yields

$$\frac{EL}{V} \sim \left[\frac{F_{0.5-4}(t_p)}{F_{1-8}(t_p)} \right]^{2.04}. \quad (6)$$

Since the *GOES* fluxes decay exponentially (at least approximately) the energy flux should also decay exponentially during the decay of the flare. This behavior is evident in the simulation results.

The plot of the total energy deposited into each thread shown in Figure 7 is rather surprising. The input energy increases during the rise phase of the flare, as expected. During the decay, however, the input energy remains relatively constant. Given the exponential decay in both the *GOES* emission and the energy flux it seems reasonable to assume that the total energy input into each thread would also decline rapidly during the decay phase. However, Equations 2 and 3 indicate that the *GOES* intensities should decay even faster than the energy flux, since the intensities are, approximately, quadratic functions of the energy flux. The *GOES* 0.5–4 to 1–8 Å ratio, which is broadly indicative of the temperature, goes as the square root of the energy flux (see Equation 6) and should therefore decay more slowly than the *GOES* intensities. This is the opposite of what is typically observed. Typically the temperature declines more rapidly than the *GOES* intensities (e.g., Sterling et al. 1997). Thus the rise in the thread volume counters, at least partially, the rapid decline in the energy flux and leads to a much slower decline in the total energy during the decay of the flare than anticipated.

Intuitively, the rise in the thread volume is largely the result of the rapid rise of the reconnection region and the corresponding increase in the thread length. In this simulation, however, the length of the threads has remained fixed. The L^{-1} scaling of the *GOES* flux Equations 2 and 3 suggest that increasing the thread length will actually accelerate the decline in the *GOES* fluxes and lead to an even more rapid increase in the thread volume. However, since the simulation parameters are computed from the residual *GOES* fluxes, the cooling of the previous threads plays an important role in determining the flare energy. As the thread length increases the conductive cooling time increases and the cooling of the thread proceeds more slowly (e.g., Cargill et al. 1995). This leads to smaller residual fluxes and potentially smaller volumes.

The nonlinearity of the flare simulation makes it difficult to determine exactly how the energy will vary when the length is properly accounted for. The rapid decline of the highest temperature emission, as indicated by the HXT L and BCS Fe XXV light curves, suggests that the energy flux declines rapidly during the decay. Given the strong dependence of the *GOES* fluxes on the energy

flux it is clear that the volume must rise rapidly during the decay of the flare. Thus it seems highly likely that the energy released during the decay phase is substantial, as indicated by these simulation results.

In this simulation assumptions have been made regarding the location and duration of the heating. We have also made assumptions about the rate at which new threads are introduced into the simulation. Recent work on impulsive heating in hydrodynamic simulations suggest that variations in the duration of the heating are the most likely to have the most significant observable consequences. The simulation algorithm yields the total energy and volume for each thread, it says nothing about the rate at which energy is released into the thread. Winebarger & Warren (2004) have shown that once the thread reaches the radiative phase of the cooling the evolution of the thread is determined largely by the total energy. During the conductive phase, in contrast, the details of the energy release, such as the heating rate, do influence the evolution of the density and temperature. The peak temperature is particularly sensitive to how impulsive the heating is. Since the HXT channels and the BCS Fe XXV line are very sensitive to the presence of very high temperature plasma we expect these light curves to discriminate between heating parameters.

To investigate this we compute another simulation where the width of the heating envelope has been set to 20 s. For this case a grid of solutions to the hydrodynamic equations are computed using this heating profile and the flare simulation is performed using the procedure outlined previously. The resulting light curves for *GOES* 0.5–4 Å, HXT M1, HXT L, and BCS Fe XXIV are shown in Figure 8. The more impulsive nature of the heating in this simulation leads to higher maximum temperatures for each thread. The higher temperatures are reflected in the light curves for the highest temperature emission. The HXT M1 channel shows greatly enhanced emission for the more impulsive heating. The impact of the shortened heating time scale becomes progressively smaller for emission formed at lower temperatures. In Figure 8 we see that the simulation with the more gentle heating (200 s) is in better agreement with the observations than the simulation with the impulsive heating.

6. Discussion

One dimensional hydrodynamic modeling represents an important link between our physical understanding of processes in the solar corona and solar observations. The details of the energy release through magnetic reconnection, for example, can be investigated with magnetohydrodynamics (MHD), but three dimensional MHD simulations generally lack the spatial resolution needed to properly track the flow of mass and energy through the solar atmosphere. This limits our ability to directly compare MHD simulation results with observation.

We have shown that it is possible to use hydrodynamic simulations to reproduce many of the salient properties of the observed light curves. Though the heating function assumed in the hydrodynamic simulation is phenomenological, these simulations do provide important constraints

on the energy release mechanism. These simulations of the Masuda flare, for example, indicate that very impulsive heating with short heating time scales (~ 20 s) would lead to the formation of very high temperature plasma. The *Yohkoh* HXT observations provide an upper bound on the plasma temperature in the bulk of the arcade and suggest that such very impulsive heating is not consistent with the available data. The simulations that are more broadly consistent with the observations have a heating time scale that is relatively long (~ 200 s), and any successful model of magnetic reconnection must reproduce this. Similarly, these simulations suggest the the rate of energy release decays slowly during the decay phase of the flare. This is potentially another important constraint on the energy release mechanism.

In addition to providing a link between the observations and the details of the energy release during a flare, these simulations also have practical applications. The changes in the solar soft X-ray and EUV irradiance during a flare, for example, perturb the Earth’s ionosphere and provide an ideal way to test our understanding of physical processes in this region of the upper atmosphere (e.g., Meier et al. 2002). Spectrally resolved EUV irradiance observations taken during solar flares are rare, however. Our simulation results provide a means for computing time-dependent soft X-ray and EUV irradiance variations associated with a flare that can be used in modeling the ionospheric response. The initial application of these modeling techniques have provided encouraging results (Huba et al. 2005).

In performing these flare simulations we have made several simplifying assumptions that reduce the computational complexity of the calculations. For example, we have assumed a constant loop length for all of the hydrodynamic simulations. This allows us to use a single grid of solutions to determine the energy and volume for each thread. Accommodating a varying loop length in the algorithm will not be difficult, but will increase the cpu time required for a simulation substantially. We have also assumed that energy transport during the initial phase of the flare is solely due to thermal conduction. In reality, bursts of hard X-rays are present during the rise phase of almost every large flare. Accounting for these hard X-ray bursts can be accomplished by computing grid of solutions for beam heated threads and partitioning the energy between in situ heating and beam heating using the observed high energy hard X-ray emission. Such modeling would provide important constraints on the partition of thermal and non-thermal heating during a flare.

This research was supported by NASA’s Sun-Earth Connection Guest Investigator program and the NRL/ONR 6.1 basic research program.

REFERENCES

- Aschwanden, M. J., & Alexander, D. 2001, *Sol. Phys.*, 204, 91
- Aschwanden, M. J., Hudson, H., Kosugi, T., & Schwartz, R. A. 1996, *ApJ*, 464, 985
- Cargill, P. J., Mariska, J. T., & Antiochos, S. K. 1995, *ApJ*, 439, 1034

- Culhane, J. L., et al. 1991, *Sol. Phys.*, 136, 89
- Doschek, G. A., Strong, K. T., & Tsuneta, S. 1995, *ApJ*, 440, 370
- Hori, K., Yokoyama, T., Kosugi, T., & Shibata, K. 1997, *ApJ*, 489, 426
- Hori, K., Yokoyama, T., Kosugi, T., & Shibata, K. 1998, *ApJ*, 500, 492
- Huba, J. D., Warren, H. P., Joyce, G., Pi, X., Iijima, B., & Coker, C. 2005, *Geophys. Res. Lett.*, in press
- Kosugi, T., et al. 1991, *Sol. Phys.*, 136, 17
- Mariska, J. T. 1987, *ApJ*, 319, 465
- Mariska, J. T., Doschek, G. A., & Bentley, R. D. 1993, *Astrophys. J.*, 419, 418
- Mariska, J. T., Emslie, A. G., & Li, P. 1989, *ApJ*, 341, 1067
- Mariska, J. T., & Zarro, D. M. 1991, *ApJ*, 381, 572
- Masuda, S., Kosugi, T., Hara, H., Sakao, T., Shibata, K., & Tsuneta, S. 1995, *PASJ*, 47, 677
- McTiernan, J. M., Fisher, G. H., & Li, P. 1999, *ApJ*, 514, 472
- Meier, R. R., et al. 2002, *Geophys. Res. Lett.*, 29, 1461
- Moore, R. L., & Labonte, B. J. 1980, in *IAU Symp. 91: Solar and Interplanetary Dynamics*, Vol. 91, 207
- Peres, G., Reale, F., Serio, S., & Pallavicini, R. 1987, *ApJ*, 312, 895
- Reale, F., Betta, R., Peres, G., Serio, S., & McTiernan, J. 1997, *A&A*, 325, 782
- Reeves, K. K., & Warren, H. P. 2002, *ApJ*, 578, 590
- Schmieder, B., Heinzl, P., Wiik, J. E., Lemen, J., Anwar, B., Kotrc, P., & Hiei, E. 1995, *Sol. Phys.*, 156, 337
- Sterling, A. C., Hudson, H. S., Lemen, J. R., & Zarro, D. A. 1997, *ApJS*, 110, 115
- Svestka, Z., Dodson-Prince, H. W., Mohler, O. C., Martin, S. F., Moore, R. L., Nolte, J. T., & Petrasso, R. D. 1982, *Sol. Phys.*, 78, 271
- Tandberg-Hanssen, E., & Emslie, A. G. 1988, *The Physics of Solar Flares* (Cambridge and New York, Cambridge University Press, 1988, 286 p.)
- Tsuneta, S., et al. 1991, *Solar Phys.*, 136, 37
- Tsuneta, S., Masuda, S., Kosugi, T., & Sato, J. 1997, *ApJ*, 478, 787

- Wang, H., Gary, D. E., Zirin, H., Kosugi, T., Schwartz, R. A., & Linford, G. 1995, ApJ, 444, L115
- Warren, H. P. 2000, ApJ, 536, L105
- Warren, H. P., & Antiochos, S. K. 2004, ApJ, 611, L49
- Warren, H. P., Bookbinder, J. A., Forbes, T. G., Golub, L., Hudson, H. S., Reeves, K., & Warshall, A. 1999, ApJ, 527, L121
- Warren, H. P., & Doschek, G. A. 2005, ApJ, 618, L157
- Winebarger, A. R., & Warren, H. P. 2004, ApJ, 610, L129

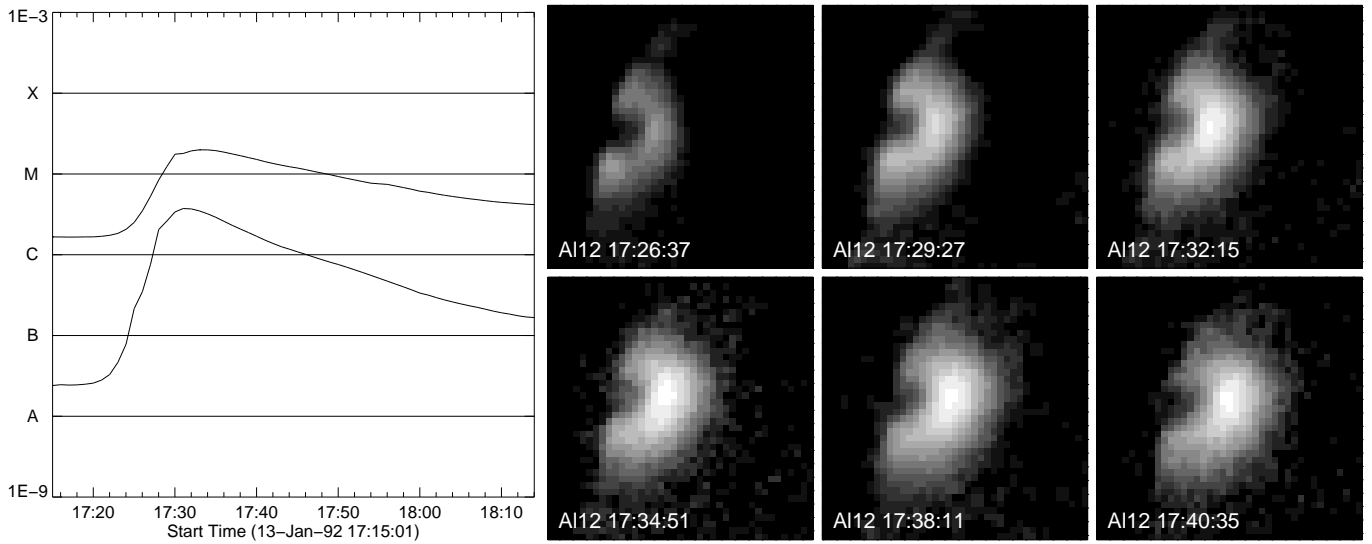


Fig. 1.— Observations of the 1992 January 13 Masuda flare. (*left panel*) *GOES* fluxes in the 1–8 and 0.5–4 Å channels. (*right panels*) SXT images of the flare arcade in the thick aluminum filter. These images span the available SXT observations. Each image is scaled logarithmically using a common intensity scaling.

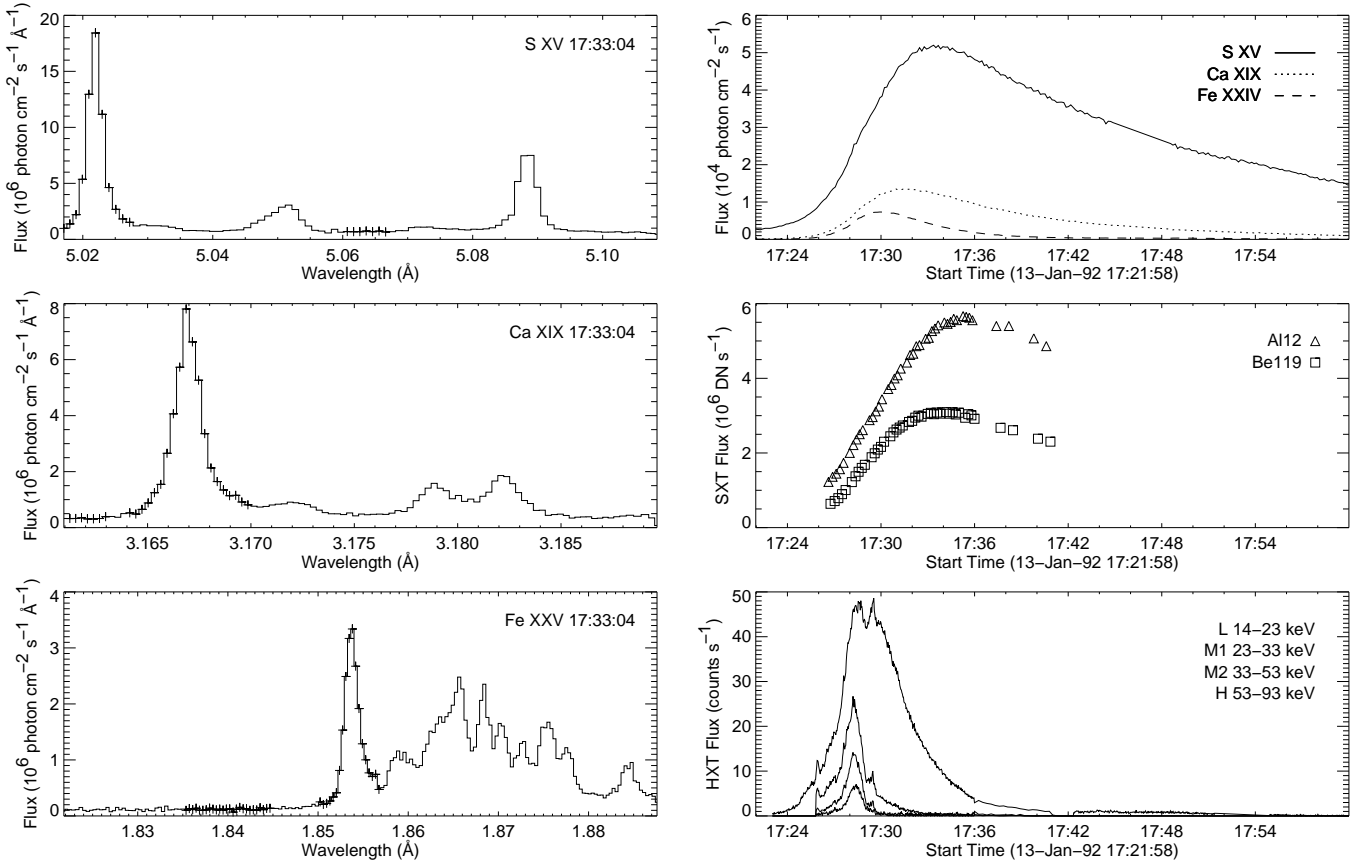


Fig. 2.— *Yohkoh* observations of the Mausa flare. (*left panels*) BCS spectra in S XV, Ca XIX, Fe XXV. The crosses indicate the spectral regions used to compute the intensities for the resonance line and the continuum. (*right panels*) Light curves for BCS, SXT, and HXT.

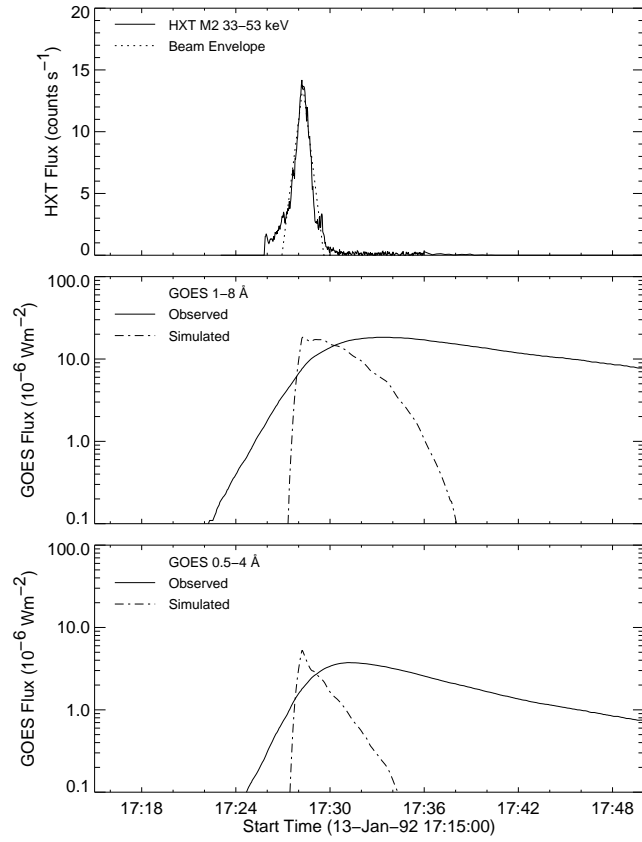


Fig. 3.— Single loop hydrodynamic modeling of the Masuda event. (*top panel*) The observed HXT hard X-ray light curve from 33–53 keV and the assumed envelope on the beam heating. (*bottom panels*) The observed and simulated GOES soft X-ray light curves.

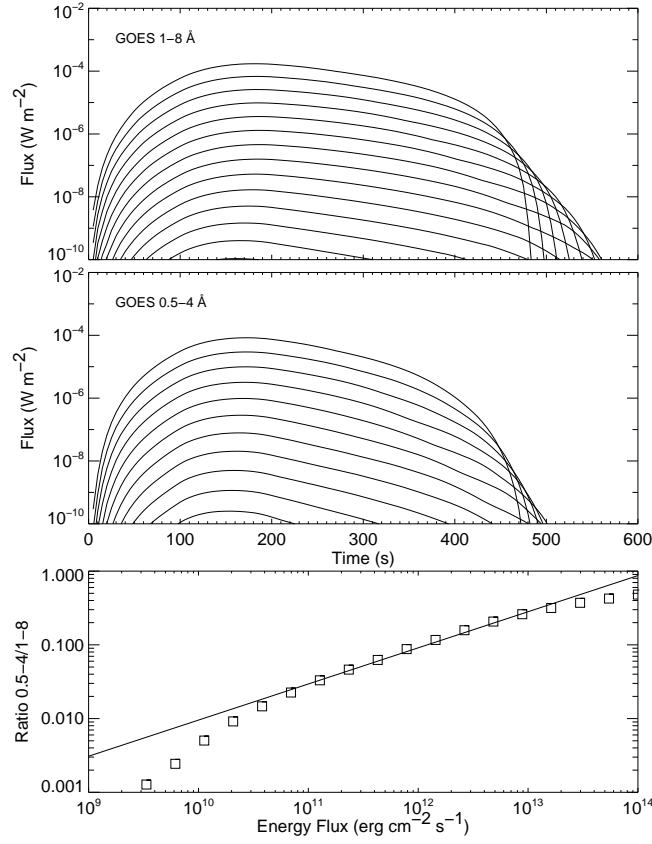


Fig. 4.— (*top panels*) Simulated *GOES* light curves as a function of time and input energy flux. (*bottom panel*) The ratio of the 0.5–4 to 1–8 Å *GOES* channels. The loop length has been fixed at approximately 39 Mm in these simulations. An area of 10^{16} cm^2 has been assumed. The solid line represents the theoretical ratio derived from the scaling laws.

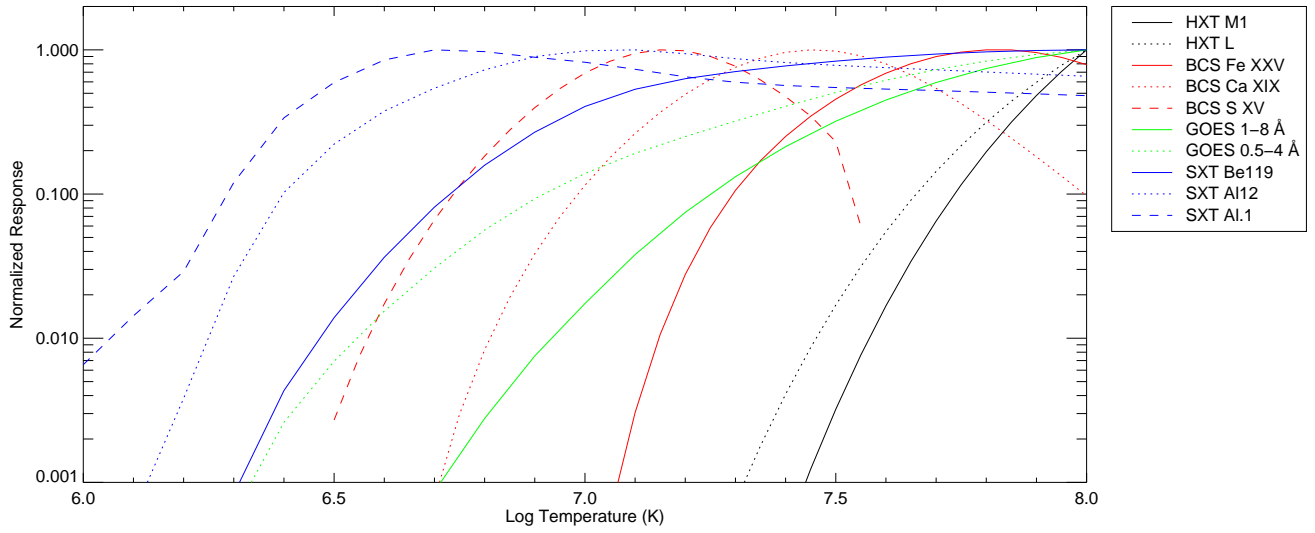


Fig. 5.— Temperature response curves the for SXT Al.1, Al12, and Be119 filters, *GOES* 0.5–4 and 1–8 Å channels, the BCS S XV, Ca XIX, and Fe XXV resonance lines, and the HXT L and M1 channels. The response in each channel has been normalized to its maximum value.

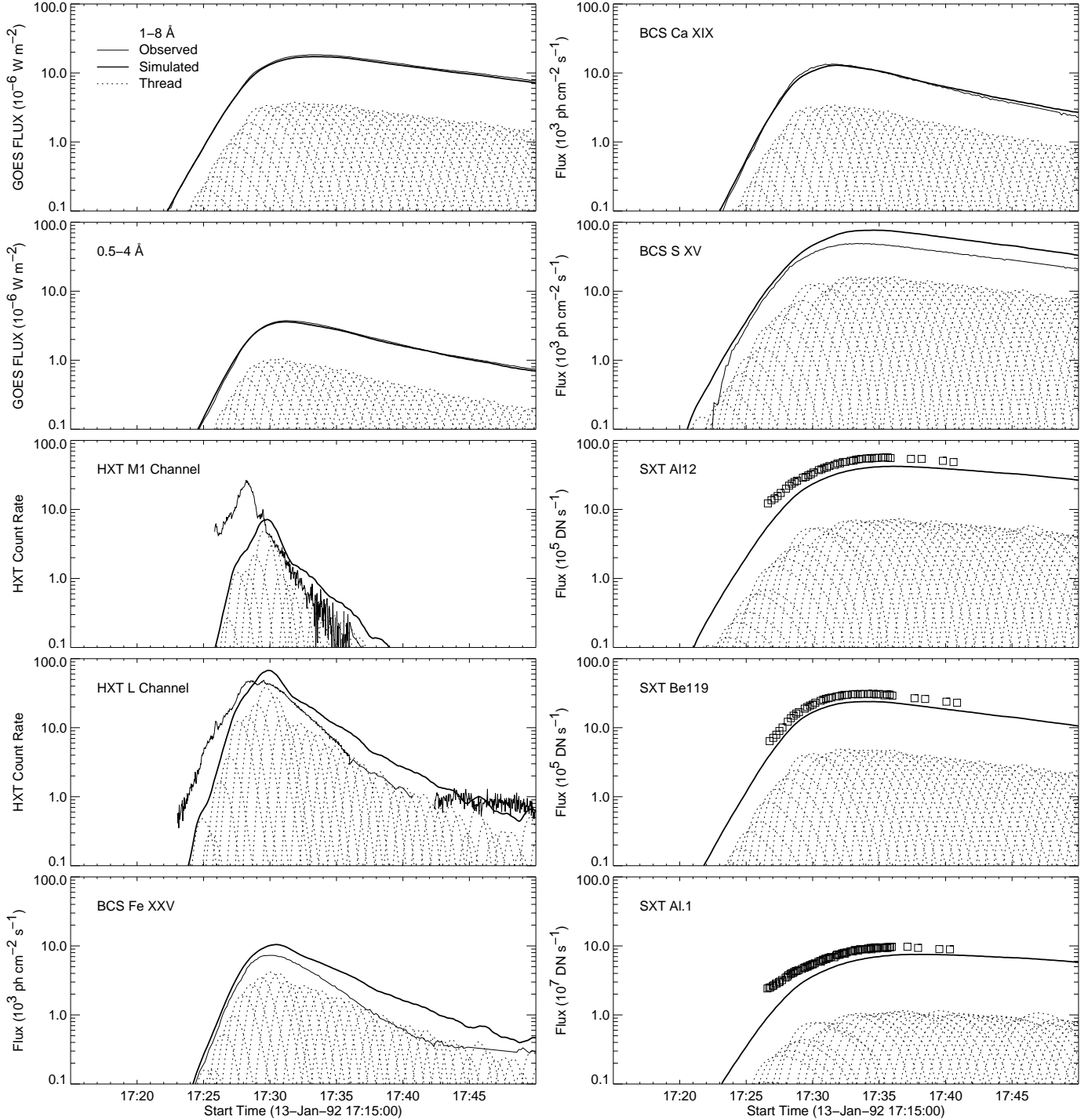


Fig. 6.— Observed and simulated light curves for the Masuda flare of 1992 January 13. No scaling factors have been applied to any of the simulated light curves. In each panel the thick solid line represents simulated light curve computed by summing the contribution of each thread. The light curves for the individual threads are indicated by the dotted lines. The observed fluxes are indicated by a thin solid line (*GOES*, *HXT*, and *BCS*) or by squares (*SXT*). See the text for a discussion of background subtraction for the observed fluxes.

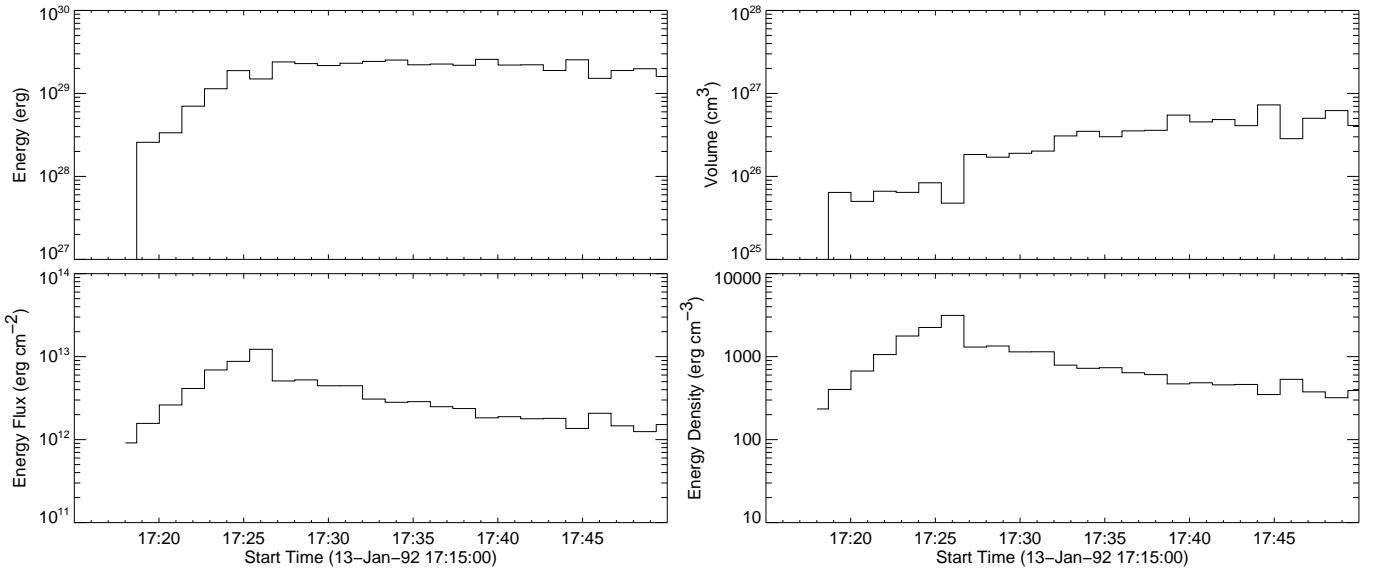


Fig. 7.— Parameters for each thread in the simulation as a function of time. Shown are the total energy, volume, average energy flux (E/A), and average energy density (E/V) for each thread. Note that the times correspond to the beginning of the heating for each thread.

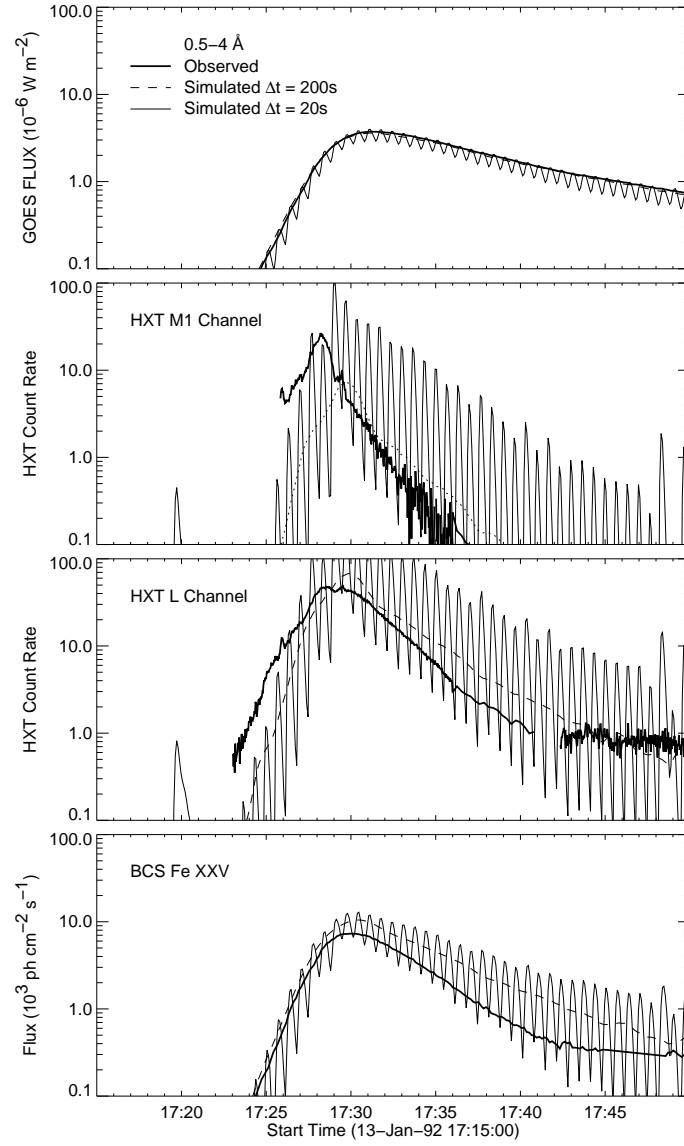


Fig. 8.— Light curves for emission formed at high temperatures for relatively gentle heating (200 s) and impulsive heating (20 s).